

# A Closed Form Solution to Natural Image Matting

Anat Levin Dani Lischinski Yair Weiss  
School of Computer Science and Engineering  
The Hebrew University of Jerusalem  
{alevin,danix,yweiss}@cs.huji.ac.il

## Abstract

*Interactive digital matting, the process of extracting a foreground object from an image based on limited user input, is an important task in image and video editing. From a computer vision perspective, this task is extremely challenging because it is massively ill-posed — at each pixel we must estimate the foreground and the background colors, as well as the foreground opacity (“alpha matte”) from a single color measurement. Current approaches either restrict the estimation to a small part of the image, estimating foreground and background colors based on nearby pixels where they are known, or perform iterative nonlinear estimation by alternating foreground and background color estimation with alpha estimation.*

*In this paper we present a closed form solution to natural image matting. We derive a cost function from local smoothness assumptions on foreground and background colors, and show that in the resulting expression it is possible to analytically eliminate the foreground and background colors to obtain a quadratic cost function in alpha. This allows us to find the globally optimal alpha matte by solving a sparse linear system of equations. Furthermore, the closed form formula allows us to predict the properties of the solution by analyzing the eigenvectors of a sparse matrix, closely related to matrices used in spectral image segmentation algorithms. We show that high quality mattes can be obtained on natural images from a small amount of user input.*

## 1. Introduction

Natural image matting and compositing is of central importance in image and video editing. Formally, image matting methods take as input an image  $I$ , which is assumed to be a composite of a foreground image  $F$  and a background image  $B$ . The color of the  $i$ -th pixel is assumed to be a linear combination of the corresponding foreground and background colors,

$$I_i = \alpha_i F_i + (1 - \alpha_i) B_i, \quad (1)$$

where  $\alpha_i$  is the pixel’s foreground opacity. In natural image matting, all quantities on the right hand side of the *compositing equation* (1) are unknown. Thus, for a 3 channel

color image, at each pixel there are 3 equations and 7 unknowns.

Obviously, this is a severely under-constrained problem, and user interaction is required to extract a good matte. Most recent methods expect the user to provide a *trimap* as a starting point; an example is shown in Figure 1(e). The trimap is a rough (typically hand-drawn) segmentation of the image into three regions: foreground (shown in white), background (shown in black) and unknown (shown in gray). Given the trimap, these methods typically solve for  $F$ ,  $B$ , and  $\alpha$  simultaneously. This is typically done by iterative nonlinear optimization, alternating the estimation of  $F$  and  $B$  with that of  $\alpha$ . In practice, this means that for good results the unknown regions in the trimap must be as small as possible. As a consequence, trimap-based approaches typically experience difficulty handling images with a significant portion of mixed pixels or when the foreground object has many holes [17]. In such challenging cases a great deal of experience and user interaction may be necessary to construct a trimap that would yield a good matte. Another problem with the trimap interface is that the user cannot directly influence the matte in the most important part of the image: the mixed pixels.

In this paper we present a new closed-form solution for extracting the alpha matte from a natural image. We derive a cost function from local smoothness assumptions on foreground and background colors  $F$  and  $B$ , and show that in the resulting expression it is possible to analytically eliminate  $F$  and  $B$ , yielding a quadratic cost function in  $\alpha$ . The alpha matte produced by our method is the global optimum of this cost function, which may be obtained by solving a sparse linear system. Since our approach computes  $\alpha$  directly and without requiring reliable estimates for  $F$  and  $B$ , a small amount of user input (such as a sparse set of scribbles) is often sufficient for extracting a high quality matte. Furthermore, our closed-form formulation enables one to understand and predict the properties of the solution by examining the eigenvectors of a sparse matrix, closely related to matrices used in spectral image segmentation algorithms. In addition to providing a solid theoretical basis for our approach, such analysis can provide useful hints to the user regarding where in the image scribbles should be placed.

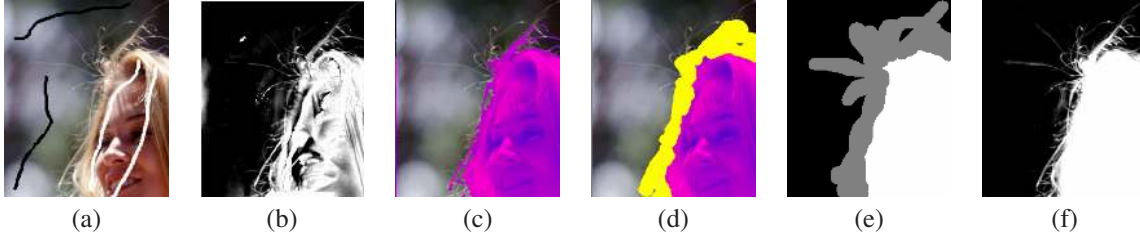


Figure 1. (a) An image with sparse constraints: white scribbles indicate foreground, black scribbles indicate background. Applying Bayesian matting to such sparse input produces a completely erroneous matte (b). Foreground extraction algorithms, such as [10, 12] produce a hard segmentation (c). An automatically generated trimap from a hard segmentation may miss fine features (d). An accurate hand-drawn trimap (e) is required in this case to produce a reasonable matte (f). (Images taken from [17])

### 1.1. Previous work

Most existing methods for natural image matting require the input image to be accompanied by a *trimap* [1, 2, 5, 6, 13, 15], labeling each pixel as foreground, background, or unknown. The goal of the method is to solve the compositing equation (1) for the unknown pixels. This is typically done by exploiting some local regularity assumptions on  $F$  and  $B$  to predict their values for each pixel in the unknown region. In the Corel KnockOut algorithm [2],  $F$  and  $B$  are assumed to be smooth and the prediction is based on a weighted average of known foreground and background pixels (closer pixels receive higher weight). Some algorithms [6, 13] assume that the local foreground and background come from a relatively simple color distribution. Perhaps the most successful of these algorithms is the Bayesian matting algorithm [6], where a mixture of oriented Gaussians is used to learn the local distribution and then  $\alpha$ ,  $F$ , and  $B$  are estimated as the most probable ones given that distribution. Such methods work well when the color distributions of the foreground and the background do not overlap, and the unknown region in the trimap is small. As demonstrated in Figure 1(b) a sparse set of constraints could lead to a completely erroneous matte. In contrast, while our approach also makes certain smoothness assumptions regarding  $F$  and  $B$ , it does not involve estimating the values of these functions until after the matte has been extracted.

The Poisson matting method [15], also expects a trimap as part of its input, and computes the alpha matte in the mixed region by solving a Poisson equation with the matte gradient field and Dirichlet boundary conditions. In the *global Poisson matting* method the matte gradient field is approximated as  $\nabla I / (F - B)$  by taking the gradient of the compositing equation, and neglecting the gradients in  $F$  and  $B$ . The matte is then found by solving for a function whose gradients are as close as possible to the approximated matte gradient field. Whenever  $F$  or  $B$  are not sufficiently smooth inside the unknown region, the resulting matte might not be correct, and additional local manipulations may need to be applied interactively to the matte gradient field in order to obtain a satisfactory solution. This interactive refinement process is referred to as *local Poisson matting*. As we shall

see, our method makes weaker assumptions on the behavior of  $F$  and  $B$ , which generally leads to more accurate mattes.

Recently, several successful approaches for extracting a foreground object from its background have been proposed [3, 10, 12]. Both approaches translate simple user-specified constraints (such as scribbles, or a bounding rectangle) into a min-cut problem. Solving the min-cut problem yields a hard binary segmentation, rather than a fractional alpha matte (Figure 1(c)). The hard segmentation could be transformed into a trimap by erosion, but this could still miss some fine or fuzzy features (Figure 1(d)). Although Rother *et al.* [12] do perform border matting by fitting a parametric alpha profile in a narrow strip around the hard boundary, this is more akin to feathering than to full alpha matting, since wide fuzzy regions cannot be handled in this manner.

Our approach is closely related to the colorization method of Levin *et al.* [9], and the random walk alpha matting method of Grady *et al.* [8]. Both of these methods propagate scribbled constraints to the entire image by minimizing a quadratic cost function. Here we apply a similar strategy, but our assumptions and cost function are modified so as to better suit the matting problem.

Another scribble-based interface for interactive matting was recently proposed by Wang and Cohen [17]. Starting from a few scribbles indicating a small number of background and foreground pixels, they use belief propagation to iteratively estimate the unknowns at every pixel in the image. While this approach has produced some impressive results, it has the disadvantage of employing an expensive iterative non-linear optimization process, which might converge to different local minima.

## 2. Derivation

For clarity of exposition we begin by deriving a closed-form solution for alpha matting of grayscale images. This solution will then be extended to the case of color images in Section 2.1.

As mentioned earlier, the matting problem is severely under-constrained. Therefore, some assumptions on the nature of  $F$ ,  $B$  and/or  $\alpha$  are needed. To derive our solution for the grayscale case we make the assumption that both  $F$  and  $B$  are approximately constant over a small window around

each pixel. Note that assuming  $F$  and  $B$  are locally smooth does not mean that the input image  $I$  is locally smooth, since discontinuities in  $\alpha$  can account for the discontinuities in  $I$ . This assumption, which will be somewhat relaxed in Section 2.1, allows us to rewrite (1) expressing  $\alpha$  as a linear function of the image  $I$ :

$$\alpha_i \approx aI_i + b, \quad \forall i \in w, \quad (2)$$

where  $a = \frac{1}{F-B}$ ,  $b = -\frac{B}{F-B}$  and  $w$  is a small image window. This linear relation is similar to the prior used in [19], and the shape recipes of [16]. Our goal in this paper will be to find  $\alpha$ ,  $a$  and  $b$  minimizing the cost function

$$J(\alpha, a, b) = \sum_{j \in I} \left( \sum_{i \in w_j} (\alpha_i - a_j I_i - b_j)^2 + \varepsilon a_j^2 \right), \quad (3)$$

where  $w_j$  is a small window around pixel  $j$ .

The cost function above includes a regularization term on  $a$ . One reason for adding this term is numerical stability. For example, if the image is constant in the  $j$ -th window,  $a_j$  and  $b_j$  cannot be uniquely determined without a prior. Also, minimizing the norm of  $a$  biases the solution towards smoother  $\alpha$  mattes (since  $a_j = 0$  means that  $\alpha$  is constant over the  $j$ -th window).

In our implementation, we typically use windows of  $3 \times 3$  pixels. Since we place a window around each pixel, the windows  $w_j$  in (3) overlap. It is this property that enables the propagation of information between neighboring pixels. The cost function is quadratic in  $\alpha$ ,  $a$  and  $b$ , with  $3N$  unknowns for an image with  $N$  pixels. Fortunately, as we show below,  $a$  and  $b$  may be eliminated from (3), leaving us with a *quadratic* cost in only  $N$  unknowns: the alpha values of the pixels.

**Theorem 1** Define  $J(\alpha)$  as

$$J(\alpha) = \min_{a,b} J(\alpha, a, b).$$

Then

$$J(\alpha) = \alpha^T L \alpha, \quad (4)$$

where  $L$  is an  $N \times N$  matrix, whose  $(i, j)$ -th entry is:

$$\sum_{k|(i,j) \in w_k} \left( \delta_{ij} - \frac{1}{|w_k|} \left( 1 + \frac{1}{\frac{\varepsilon}{|w_k|} + \sigma_k^2} (I_i - \mu_k)(I_j - \mu_k) \right) \right) \quad (5)$$

Here  $\delta_{ij}$  is the Kronecker delta,  $\mu_k$  and  $\sigma_k^2$  are the mean and variance of the intensities in the window  $w_k$  around  $k$ , and  $|w_k|$  is the number of pixels in this window.

*Proof:* Rewriting (3) using matrix notation we obtain

$$J(\alpha, a, b) = \sum_k \left\| G_k \begin{bmatrix} a_k \\ b_k \end{bmatrix} - \bar{\alpha}_k \right\|^2, \quad (6)$$

where for every window  $w_k$ ,  $G_k$  is defined as a  $(|w_k| + 1) \times 2$  matrix. For each  $i \in w_k$ ,  $G_k$  contains a row of the form  $[I_i, 1]$ , and the last row of  $G_k$  is of the form  $[\sqrt{\varepsilon}, 0]$ . For a given matte  $\alpha$  we define  $\bar{\alpha}_k$  as a  $(|w_k| + 1) \times 1$  vector, whose entries are  $\alpha_i$  for every  $i \in w_k$ , and whose last entry is 0. The elements in  $\bar{\alpha}_k$  and  $G_k$  are ordered correspondingly.

For a given matte  $\alpha$  the optimal pair  $a_k^*, b_k^*$  inside each window  $w_k$  is the solution to the least squares problem:

$$(a_k^*, b_k^*) = \operatorname{argmin} \left\| G_k \begin{bmatrix} a_k \\ b_k \end{bmatrix} - \bar{\alpha}_k \right\|^2 \quad (7)$$

$$= (G_k^T G_k)^{-1} G_k^T \bar{\alpha}_k \quad (8)$$

Substituting this solution into (6) and denoting  $\bar{G}_k = I - G_k(G_k^T G_k)^{-1} G_k^T$  we obtain

$$J(\alpha) = \sum_k \bar{\alpha}_k^T \bar{G}_k^T \bar{G}_k \bar{\alpha}_k,$$

and some further algebraic manipulations show that the  $(i, j)$ -th element of  $\bar{G}_k^T \bar{G}_k$  may be expressed as:

$$\delta_{ij} - \frac{1}{|w_k|} \left( 1 + \frac{1}{\frac{\varepsilon}{|w_k|} + \sigma_k^2} (I_i - \mu_k)(I_j - \mu_k) \right).$$

Summing over  $k$  yields the expression in (5).  $\square$

## 2.1. Color Images

A simple way to apply the cost function to color images is to apply the gray level cost to each channel separately. Alternatively we can replace the linear model (2), with a 4D linear model:

$$\alpha_i \approx \sum_c a^c I_i^c + b, \quad \forall i \in w \quad (9)$$

The advantage of this combined linear model is that it relaxes our previous assumption that  $F$  and  $B$  are constant over each window. Instead, as we show below, it is enough to assume that in a small window each of  $F$  and  $B$  is a linear mixture of two colors; in other words, the values  $F_i$  in a small window lie on a single line in the RGB color space:  $F_i = \beta_i F_1 + (1 - \beta_i) F_2$ , and the same is true for the background values  $B_i$ . In what follows we refer to this assumption as the *color line model*.

Such a model is useful since it captures, for example, the varying shading on a surface with a constant albedo. Another example is a situation where the window contains an edge between two uniformly colored regions both belonging to the background or the foreground. In figure 2 we illustrate this concept, by plotting local *RGB* distributions from a real image. Furthermore, Omer and Werman [11] demonstrated that in many natural images the pixel colors in RGB space tend to form a relatively small number of elongated clusters. Although these clusters are not straight lines, their skeletons are roughly linear locally.

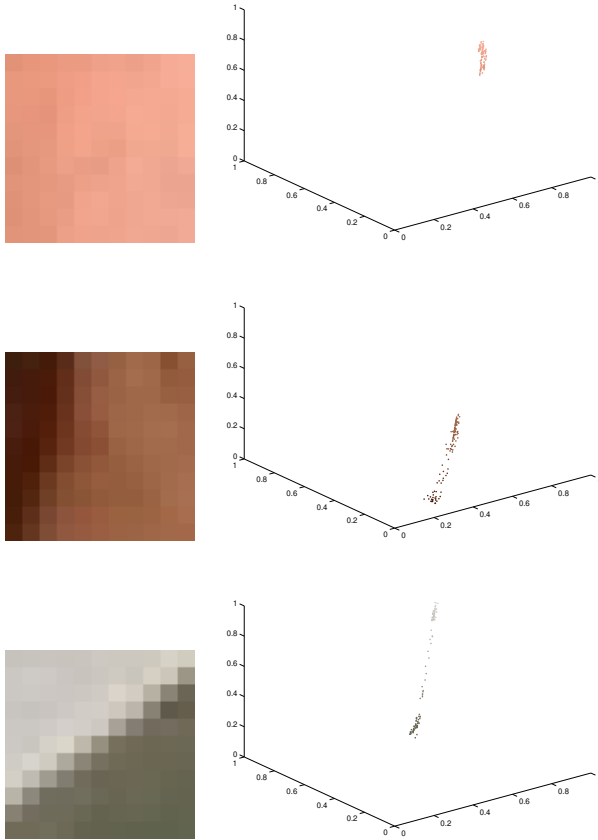
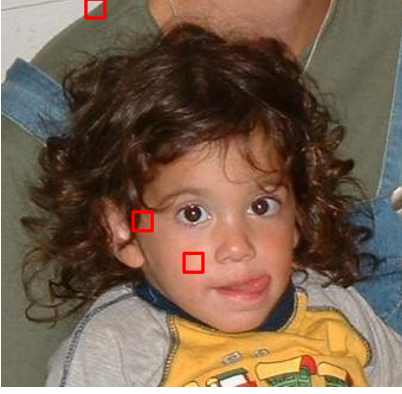


Figure 2. Local patches selected from a real image and the *RGB* plots of their color distributions.

**Theorem 2** *If the foreground and background colors in a window satisfy the color line model we can express*

$$\alpha_i = \sum_c a^c I_i^c + b, \quad \forall i \in w.$$

*Proof:* Substituting into (1) the linear combinations  $F_i = \beta_i^F F_1 + (1 - \beta_i^F) F_2$  and  $B_i = \beta_i^B B_1 + (1 - \beta_i^B) B_2$ , where  $F_1, F_2, B_1, B_2$  are constant over a small window, we obtain:

$$I_i^c = \alpha_i (\beta_i^F F_1^c + (1 - \beta_i^F) F_2^c) + (1 - \alpha_i) (\beta_i^B B_1^c + (1 - \beta_i^B) B_2^c).$$

Let  $H$  be a  $3 \times 3$  matrix whose  $c$ -th row is  $[F_2^c + B_2^c, F_1^c - F_2^c, B_1^c - B_2^c]$ . Then the above may be rewritten as:

$$H \begin{bmatrix} \alpha_i \\ \alpha_i \beta_i^F \\ (1 - \alpha_i) \beta_i^B \end{bmatrix} = I_i - B_2,$$

where  $I_i$  and  $B_2$  are  $3 \times 1$  vectors representing 3 color channels. We denote by  $a^1, a^2, a^3$  the elements in the first row of  $H^{-1}$ , and by  $b$  the scalar product of first row of  $H^{-1}$  with the vector  $B_2$ . We then obtain  $\alpha_i = \sum_c a^c I_i^c + b$ .  $\square$

Using the 4D linear model (9) we define the following cost function for matting of *RGB* images:

$$J(\alpha, a, b) = \sum_{j \in I} \left( \sum_{i \in w_j} \left( \alpha_i - \sum_c a_j^c I_i^c - b_j \right)^2 + \varepsilon \sum_c a_j^c{}^2 \right) \quad (10)$$

Similarly to the grayscale case,  $a^c$  and  $b$  can be eliminated from the cost function, yielding a quadratic cost in the  $\alpha$  unknowns alone:

$$J(\alpha) = \alpha^T L \alpha. \quad (11)$$

Here  $L$  is an  $N \times N$  matrix, whose  $(i, j)$ -th element is:

$$\sum_{k|(i,j) \in w_k} \left( \delta_{ij} - \frac{1}{|w_k|} (1 + (I_i - \mu_k)(\Sigma_k + \frac{\varepsilon}{|w_k|} I_3)^{-1} (I_j - \mu_k)) \right) \quad (12)$$

where  $\Sigma_k$  is a  $3 \times 3$  covariance matrix,  $\mu_k$  is a  $3 \times 1$  mean vector of the colors in a window  $w_k$ , and  $I_3$  is the  $3 \times 3$  identity matrix.

We refer to the matrix  $L$  in equations (5) and (12) as the *matting Laplacian*. Note that the elements in each row of  $L$  sum to zero, and therefore the nullspace of  $L$  includes the constant vector. If  $\varepsilon = 0$  is used, the nullspace of  $L$  also includes every color channel of  $I$ .

Apart from the mathematical justification, the intuition behind our cost function is that locally, the alpha can be represented as a linear combination of the image. Figure 3 demonstrates 3 representative cases. The first example is a window with rather uniform foreground and background colors. In this case the alpha has a strong normalized correlation with the image and it can be generated by multiplying one of the color channels by a scale factor and adding a constant. The second example demonstrates a constant alpha window. Regardless of the complexity of the image texture in this window, we can generate the constant alpha if we multiply the image by zero and add a constant. This trivial case is important, as it explains some of the model power. As a typical  $\alpha$ -matte is constant (0 or 1) in most image windows, the matte in such windows can be expressed as a linear function of the image in a trivial way, regardless of the exact color distribution, and whatever the color line model holds or not. Finally we present a window with non uniform alpha, where in addition, the background contains an edge. Since the edge contrasts in the different color

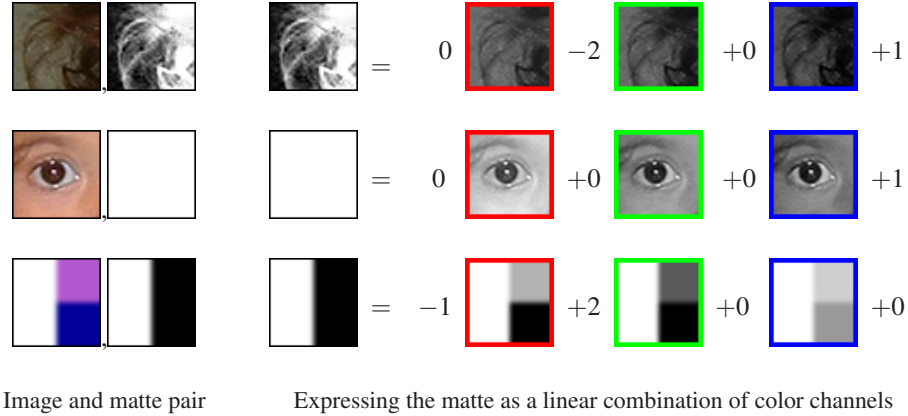


Figure 3. Local linear relations between alpha windows and image windows.

channels are different, by scaling the color channels appropriately we can actually cancel the background edge.

### 3. Constraints and User Interface

In our system the user-supplied constraints on the matte are provided via a scribble-based GUI. The user uses a background brush (black scribbles in our examples) to indicate background pixels ( $\alpha = 0$ ) and a foreground brush (white scribbles) to indicate foreground pixels ( $\alpha = 1$ ).

To extract an alpha matte matching the user’s scribbles we solve for

$$\alpha = \operatorname{argmin} \alpha^T L \alpha + \lambda (\alpha^T - b_S^T) D_S (\alpha - b_S) \quad (13)$$

where  $\lambda$  is some large number,  $D_S$  is a diagonal matrix whose diagonal elements equal 1 for scribbled pixels and 0 for all other pixels, and  $b_S$  is the vector containing the scribble values in the scribbled pixels and 0 for all other pixels.

Since the above cost is quadratic the minimization can be done by differentiating it and setting the derivatives to 0. This is equivalent to solving the following sparse linear system:

$$(L + \lambda D_S) \alpha = \lambda b_S \quad (14)$$

**Theorem 3** *Let  $I$  be an image formed from  $F$  and  $B$  according to the compositing equation (eq 1), and let  $\alpha^*$  denote the true alpha matte. If  $F$  and  $B$  satisfy the color line model in every local window  $w_k$ , and if the user-specified constraints  $S$  are consistent with  $\alpha^*$ , then  $\alpha^*$  is an optimal solution for the system (13), where  $L$  is constructed with  $\varepsilon = 0$ .*

*Proof:* Since  $\varepsilon = 0$ , if the color line model is satisfied in every window  $w_k$ , it follows from the definition (10) that  $J(\alpha^*, a, b) = 0$ , and therefore  $J(\alpha^*) = \alpha^{*T} L \alpha^* = 0$ .  $\square$

We demonstrate this in figure 4. The first image (figure 4(a)) is a synthetic example that was created by compositing computer-simulated (monochromatic) smoke over

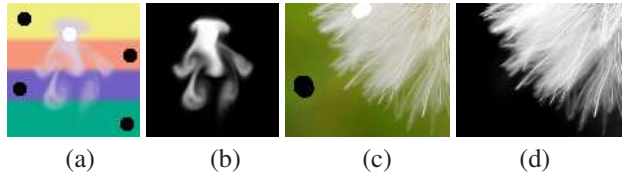


Figure 4. Matting examples. (a,c) Input images with scribbles. (b,d) Extracted mattes.

a simple background with several color bands, which satisfies the color line model. The black and white scribbles show the input constraints. The matte extracted by our method (figure 4(b)) is indeed *identical* to the ground truth matte. The second example (figure 4(c)) is a real image, with fairly uniform foreground and background colors. By scribbling only two black and white points, a high quality matte was extracted (figure 4(d)).

The above theorem is not an if-and-only-if theorem, and it should not be deduced that any solution to the quadratic cost function is the correct matte, since the minimum of the cost may not be unique. This is due to the fact that the nullspace of  $L$  may contain multiple solutions and to ensure that the true solution will be selected, the user will need to provide a sufficient number of scribbles. For example, constraining the system to output the true matte in figure 4(a), required a scribble on every connected component.

#### 3.1. Additional Scribbling Brushes

To provide the user with more flexible control over the output we add additional types of brushes for specifying constraints at regions containing mixed pixels. One simple constraint may be set by explicitly specifying the values of  $F$  and  $B$  under the scribble (by cloning them from other locations in the image). This gives a constraint on  $\alpha$  in the scribbled area, computable directly from the compositing equation (eq. 1). Another constraint type is when the artist indicates that  $F$  and  $B$  are *constant but unknown* within the scribble. This adds to the system a constraint of the type in

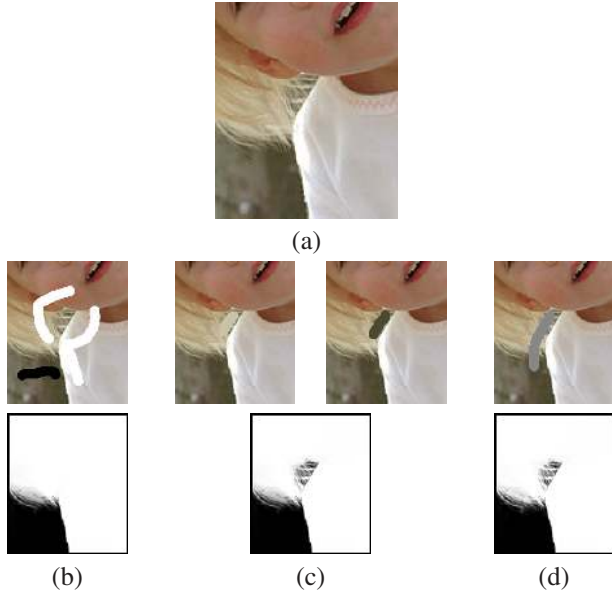


Figure 5. Using additional scribbling brushes. (a) Input image. (b) Simple black and white scribbles. (c) Scribbling foreground and background colors explicitly. (d) Marking wider neighborhoods.

equation 9, except that the window area is larger than  $3 \times 3$  and includes all of the pixels under the scribble.

The usage of these two brushes is illustrated in figure 5. If only black and white scribbles are used (fig 5(a)), there is no way to specify background constraints for the parts of the background partially visible through the fine gaps in the hair. As a result these gaps are not captured by the recovered matte (fig 5(b)). To overcome this, the user may pick some blond and brown colors from the neighboring pixels (fig 5(c)) and specify them as the foreground and background colors in that region. The matte produced this way succeeds in capturing the partial visibility of the background. Alternatively, the user may place a scribble (gray scribble in figure 5(d)) indicating that this area should be treated as a single large neighborhood, causing the brown pixels showing through the hair to be treated the same as the brown pixels outside. In the results section we show that these additional brushes are also useful for the challenging tasks of extracting shadows and smoke.

#### 4. Parameters Evaluation

To gain some understanding of our system, we illustrate here the effect of the different parameters on the alpha reconstruction.

First we demonstrate the effect of  $\epsilon$ , which weights the regularization term on  $a$  in eq. 3. There are two reasons for having this parameter. The first reason is numerical stability. For example, if the image is constant in the  $j$ -th window,  $a_j$  and  $b_j$  cannot be uniquely determined without a prior. Also, minimizing the norm of  $a$  biases the solution towards smoother  $\alpha$  mattes (since  $a_j = 0$  means that  $\alpha$  is

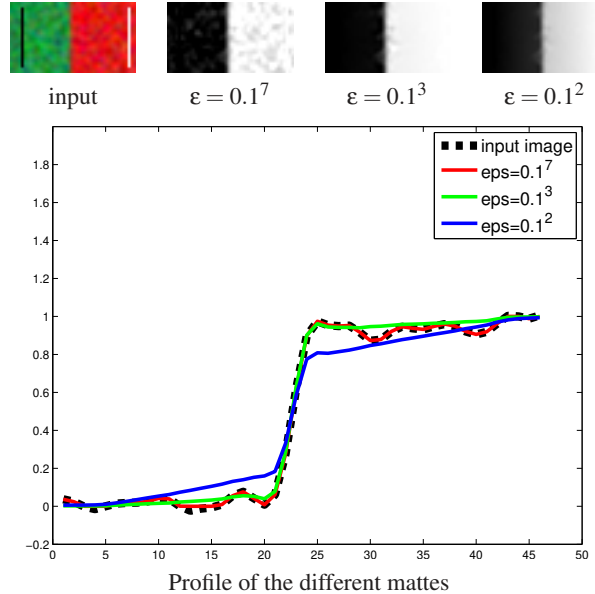


Figure 6. Computing a matte using different  $\epsilon$  values.

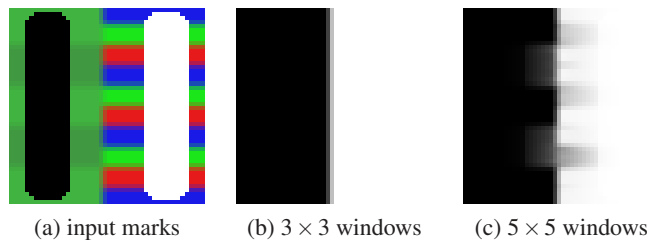


Figure 7. Computing a matte using different window sizes.

constant over the  $j$ -th window). In figure 6 we demonstrate the effect of  $\epsilon$ . Our input image consists of two noisy areas, and was scribbled with two vertical lines. In fig 6 we show three different mattes that were obtained using three different epsilon values. We also plot the different mattes using a one-dimensional profile of one of the rows. For comparison we also plot the profile of the input image scaled to the  $[0, 1]$  range. We can see that when  $\epsilon$  is small the sharpness of the recovered matte matches the profile of the edge in the input image, but the recovered alpha captures the image noise as well. For large  $\epsilon$  values the image noise is indeed ignored, but the recovered alpha is over-smoothed. In our implementation we usually used  $\epsilon = 0.1^7$  to  $0.1^5$  (as normal real images are not as noisy as the above example).

Figure 6 demonstrates the fact that  $\epsilon$  is an important parameter in our system, which controls the amount of noise versus the amount of smoothing in the solution. If  $\epsilon \rightarrow 0$  is used, the algorithm will have a problem to output constant mattes in textured regions. Yet, many of the theoretical results we were able to prove in this paper, hold only for the case  $\epsilon = 0$ .

Another parameter which affects the results is the window size. We usually construct the matting Laplacian using

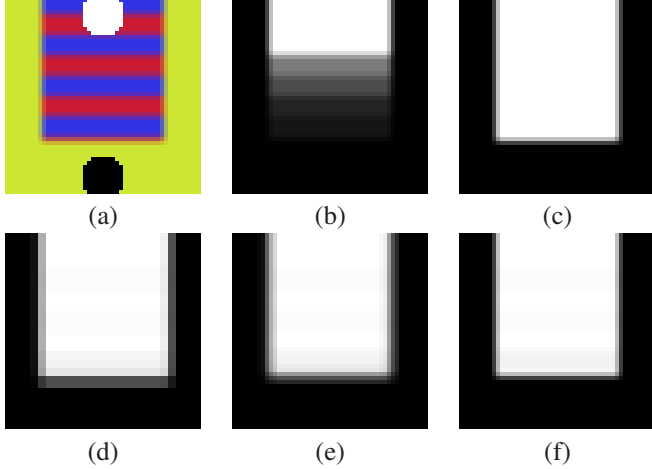


Figure 8. Computing a matte using different window sizes. (a) Input marks. (b)  $3 \times 3$  windows. (c)  $5 \times 5$  windows. (d)  $3 \times 3$  windows computed at coarser resolution. (e) Simple interpolation of (d). (f) Interpolating the  $a, b$  parameters of (d) and applying them on the finer image.

$3 \times 3$  windows. Using wider windows is more stable when the color lines model holds, but the chance of having windows deviating from the color lines model grows when the windows are wider. This is illustrated in figure 7. The matte of the image was recovered using both  $3 \times 3$  and  $5 \times 5$  windows. While the  $3 \times 3$  matte is good, the  $5 \times 5$  matte contains artifacts. The reason is that some of  $5 \times 5$  windows deviate from the color lines model since their areas cover colors of three different background strips, while the  $3 \times 3$  windows are small enough and their areas do not cover more than two strips. On the other hand, in figure 8 the fact that  $5 \times 5$  windows can cover three different strips is useful as that helps the constraint set by the white scribble to propagate to the entire striped texture region (fig 8(c)). (Despite the fact that 2 blue pixels in different strips are not direct neighbors, they are neighbors in the induced graph due to the fact that the window is wide enough). Such propagation does not occur when using  $3 \times 3$  windows (fig 8(b)).

Even in cases in which wider windows are useful, their usage increases computation time since the resulting system is less sparse. To overcome this, we consider the linear coefficients (eq. 9) that relate an alpha matte to an image. The coefficients obtained using wide windows on a fine resolution image are similar to those obtained with smaller windows on a coarser image. Therefore we can solve for the alpha matte using  $3 \times 3$  windows on a coarse image and compute the linear coefficients which relate it to the coarse image. We then interpolate the linear coefficients and apply them on a finer resolution image. The alpha matte obtained using this approach is similar to the one that would have been obtained by solving the matting system directly on the fine image with wider windows. To demonstrate this, fig. 8(d) shows the alpha matte that was obtained when  $3 \times 3$

windows were used on the image of fig. 8(a) after down-sampling it by a factor of 2. If we just upsample this alpha matte by a factor of 2 we will get a blurred alpha as in fig. 8(e). On the other hand if we compute the  $a, b$  values relating the small alpha (fig. 8(d)) to the image, upsample them and apply them to the finer resolution image, we get the sharp matte in fig. 8(f), which is almost identical to the alpha in fig. 8(c), obtained using  $5 \times 5$  windows.

## 5. Spectral Analysis

The matting Laplacian matrix  $L$  is a symmetric semi-definite matrix, as evident from theorem 1 and its proof. This matrix may also be written as  $L = D - W$ , where  $D$  is a diagonal matrix  $D(i, i) = \sum_j W(i, j)$  and  $W$  is a symmetric matrix, whose off-diagonal entries are defined by (12). Thus, the matrix  $L$  has the same form as the *graph Laplacian* used in spectral methods for segmentation, but with a novel affinity function given by (12). For comparison, the typical way to define the affinity function (e.g., in normalized cuts image segmentation algorithms [14]) is to set

$$W_G(i, j) = e^{-\|I_i - I_j\|^2 / \sigma^2}, \quad (15)$$

where  $\sigma$  is a global constant (typically chosen by hand). This affinity is large for nearby pixels with similar colors and approaches zero when the color difference is much greater than  $\sigma$ . The random walk matting algorithm [8] has used a similar affinity function for the matting problem, but the color distance between two pixels was taken after applying a linear transformation to their colors. The transformation is image-dependent and is estimated using a manifold learning technique.

In contrast, by rewriting the matting Laplacian as  $L = D - W$  we obtain the following affinity function, which we refer to as “the matting affinity”:

$$W_M(i, j) = \sum_{k|(i,j) \in w_k} \frac{1}{|w_k|} \left( 1 + (I_i - \mu_k)(\Sigma_k + \frac{\epsilon}{|w_k|} I_3)^{-1} (I_j - \mu_k) \right) \quad (16)$$

We note that by using the term *affinity* here, we somewhat extend its conventional usage. This is because the matting affinity can also take negative values, while standard affinities are usually non negative.

To compare the two affinity functions  $W_G$  and  $W_M$  we examine the eigenvectors of the corresponding Laplacians, since these eigenvectors are used by spectral segmentation algorithms for partitioning images.

Figure 9 shows the second smallest eigenvector (the first smallest eigenvector is the constant image in both cases) for both Laplacian matrices, on 3 example images. For the matting affinity, we present eigenvectors with two  $\epsilon$  values, a small  $\epsilon \rightarrow 0$  and a larger one. The first example is a simple image with concentric circles of different color. In this case the boundaries between regions are very simple, and all Laplacians capture the transitions correctly.

The second example is an image of a peacock. The global  $\sigma$  eigenvector (used by standard spectral clustering algorithms) fails to capture the complex fuzzy boundaries between the peacock’s tail feathers and the background. In contrast, the matting Laplacian’s eigenvector (constructed using  $\varepsilon = 0.1^5$ ) separates the peacock from the background very well, as this Laplacian explicitly encodes fuzzy cluster assignments. When the matting Laplacian is constructed using  $\varepsilon = 0.1^7$  the eigenvector is similar to the input image and captures the bush’s texture as well. The last example is the noisy edge of figure 6. In this case  $\varepsilon = 0.1^7$  captures all image noise and a larger  $\varepsilon$  is able to ignore some of the noise. However, when  $\sigma$  is appropriately set, the global  $\sigma$  eigenvector is capturing an ideal step edge. This step edge is an excellent result if the goal is obtaining a hard segmentation, but if we are interested in a matte, we probably want an edge whose smoothness is proportional to the smoothness of the edge in the input image, so the matting eigenvector might be more appropriate. Thus, designing a good matting affinity is not equivalent to designing a good affinity for hard segmentation.

### 5.1. The eigenvectors as guides

While the matting problem is ill-posed without some user input, the matting Laplacian matrix contains a lot of information on the image even before any scribbles have been provided, as demonstrated in the previous section.

This suggests that looking at some of the smallest eigenvectors of the matting Laplacian can guide the user *where to place scribbles*. For example, the extracted matte tends to be piecewise constant in the same regions where the smallest eigenvectors are piecewise constant. If the values inside a segment in the eigenvector image are coherent, a single scribble within such a segment should suffice to propagate the desired value to the entire segment. On the other hand, areas where the eigenvector’s values are less coherent correspond to more “difficult” regions in the image, suggesting that more scribbling efforts might be required there. We note, however, that a basic strategy for scribble placing is just to examine the input image and place scribbles on regions with different colors. This is also evident by the fact that when the matting Laplacian is constructed using  $\varepsilon = 0$ , the nullspace of the matting Laplacian will contain the 3 color channels.

Figure 10 illustrates how a scribbling process may be guided by the eigenvectors. By examining the two smallest eigenvectors (fig 10(a-b)) we placed a scribble inside each region exhibiting coherent eigenvector values (fig 10(c)). The resulting matte is shown in fig 10(d). Note that the scribbles in fig 10(c) were our first, and single attempt to place scribbles on this image.

Stated somewhat more precisely, the alpha matte may be predicted by examining some of the smaller eigenvectors of the matting Laplacian, since an optimal solution to (13) will be to a large degree spanned by the smaller eigenvectors.

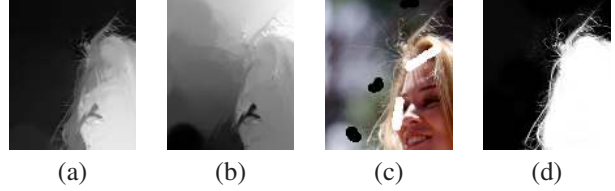


Figure 10. Smallest eigenvectors (a-b) are used for guiding scribble placement (c). The resulting matte is shown in (d).

In fact, it is possible to bound the weight that the optimal solution will assign to larger eigenvectors, as a function of the ratios of the corresponding eigenvalues.

**Theorem 4** *Let  $v_1, \dots, v_N$  be the eigenvectors of the matting Laplacian (12) with eigenvalues  $\lambda_1 \leq \lambda_2 \leq \dots \leq \lambda_N$ . Let  $S$  be the subset of scribbled pixels, with scribble values  $s_i$ ,  $i \in S$ . We denote by  $x(S)$  the restriction of the vector  $x$  to the scribbled pixels (so that  $x(S)$  is an  $|S|$  dimensional vector). Let  $\alpha$  be the optimal matte and suppose  $\alpha$  is expressed with respect to the eigenvectors basis as:  $\alpha = \sum_{k=1}^N a_k v_k$*

*If the scribbles are spanned by the  $K$  smallest eigenvectors  $s(S) = \sum_{k=1}^K b_k v_k(S)$ , then for every  $j > K$ :*

$$a_j^2 \leq \frac{\sum_{k=1}^K b_k^2}{\lambda_j} \leq \frac{\|b\|^2 \lambda_K}{\lambda_j}$$

*Proof:* Let  $\beta = \sum_{k=1}^K b_k v_k$ . Then  $\beta$  satisfies  $\beta(S) = s(S)$ . Since  $\alpha$  is the optimal solution  $\alpha = \operatorname{argmin} \alpha^T L \alpha$ , s.t.  $\alpha(S) = s(S)$ , we must have that  $\alpha^T L \alpha \leq \beta^T L \beta$ . Since the Laplacian matrix  $L$  is positive semi-definite, the eigenvectors  $v_1, \dots, v_N$  are orthogonal. Therefore,

$$\alpha^T L \alpha = \sum_{k=1}^N a_k^2 \lambda_k \tag{17}$$

$$\beta^T L \beta = \sum_{k=1}^K b_k^2 \lambda_k \tag{18}$$

and as a result for every  $j$ :  $a_j^2 \lambda_j \leq \sum_{k=1}^K b_k^2 \leq \|b\|^2 \lambda_K$ .  $\square$

**Corollary 1** *If the scribbles are spanned by the nullspace of  $L$  the optimal solution will also lie in the nullspace of  $L$ .*

*Proof:* Let  $K$  be the dimension of the nullspace. Using the previous theorem’s notation, for every  $j > K$ ,  $a_j^2 \leq \|b\|^2 \lambda_K = 0$ , and the optimal solution is spanned by the  $K$  nullspace eigenvectors.  $\square$

The above implies that the smoothness of the recovered alpha matte will tend to be similar to that of the smallest eigenvectors of  $L$ .

## 6. Optimization

The optimization problem defined in eq. 13 is one of minimizing a quadratic cost function subject to linear constraints, and the solution can therefore be found by solving a sparse set of linear equations.



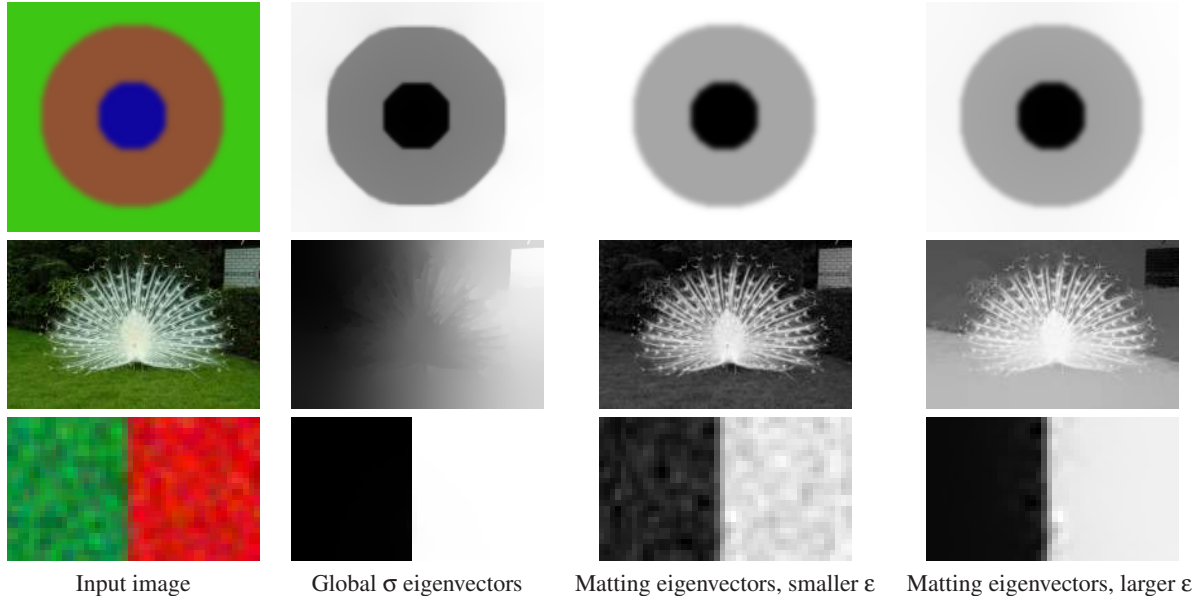


Figure 9. Smallest eigenvectors of the different Laplacians.

For the results shown here we solve the linear system using Matlab’s direct solver (the “backslash” operator), which takes 20 seconds for a 200 by 300 image on a 2.8GHz CPU. Processing large images using the Matlab solver is impossible due to memory limitations. To overcome this we use a coarse-to-fine scheme. We downsample the image and the scribbles and solve at a lower resolution. The recovered alpha matte is then interpolated to the finer resolution, alpha values are thresholded and pixels with alpha close to 0 or 1 are treated as constrained in the finer resolution. Constrained pixels may be eliminated from the system, reducing the system size. For that, we note that within the constrained areas there is no need to enforce the local linear models. Therefore, when computing the matting Laplacian matrix (equations 5,12), we sum only windows  $w_k$  which include at least one unconstrained pixel. Aside for efficiency, thresholding alpha values close to 0 or 1 is also useful in avoiding over-smoothed  $\alpha$ -mattes, and we used this trick to produce the results in figure 15(f,g).

Apart from the matlab solver, we note that solving linear systems with this structure is a well studied problem [9, 8]. We have also implemented a multigrid solver for matte extraction. The multigrid solver runs in a couple of seconds even on very large images, but with a small degradation in matte quality. Therefore, a multigrid solver enables the system to operate as an interactive tool. The user can place scribbles, examine the resulting matte and add scribbles in image areas which require further refinement.

The eigenvectors of the matting Laplacian depend only on the input image, and are independent of the user’s scribbles. It is not necessary to compute them, unless the user wishes to use them for guidance in scribble placement, as

described earlier. In this case, they only need to be computed once, possibly as part of the initialization that takes place when a new image is loaded. Recently, there has been much research of efficient methods for computation of eigenvectors (e.g., [4]), partly in response to the growing interest in normalized cuts image segmentation and other spectral clustering methods.

## 7. Reconstructing $F$ and $B$

Having solved for  $\alpha$  it is also usually necessary to reconstruct  $F$ , and in some cases also  $B$ . One approach for reconstructing  $F$  and  $B$  is to solve equation 9 for the optimal  $a, b$  given  $\alpha$  (this is a least squares problem). However, in order to extract  $F$  and  $B$  from  $a, b$  there is an additional matting parameter that should be recovered ( $\beta$  in the proof of theorem 2). For complex foreground and background patterns such a reconstruction may produce noisy results, and therefore we solve for  $F$  and  $B$  using the compositing equation, introducing some explicit smoothness priors on  $F$  and  $B$ . The smoothness priors are stronger in the presence of matte edges. Specifically, we minimize a system of the form:

$$\min \sum_{i \in I} \sum_c \left( \alpha_i F_i^c + (1 - \alpha_i) B_i^c - I_i^c \right)^2 + |\alpha_{i_x}| \left( (F_{i_x}^c)^2 + (B_{i_x}^c)^2 \right) + |\alpha_{i_y}| \left( (F_{i_y}^c)^2 + (B_{i_y}^c)^2 \right) \quad (19)$$

where  $F_{i_x}^c, F_{i_y}^c, B_{i_x}^c,$  and  $B_{i_y}^c$  are the  $x$  and  $y$  derivatives of  $F^c$  and  $B^c$ , and  $\alpha_{i_x}, \alpha_{i_y}$  are the matte derivatives. We note that for a fixed  $\alpha$  the cost in eq. 19 is quadratic and its minimization may be done by solving a sparse set of linear equations. Given the solution of  $F$  and  $B$  the  $\alpha$  solution can be further refined, but in practice we have observed this is not

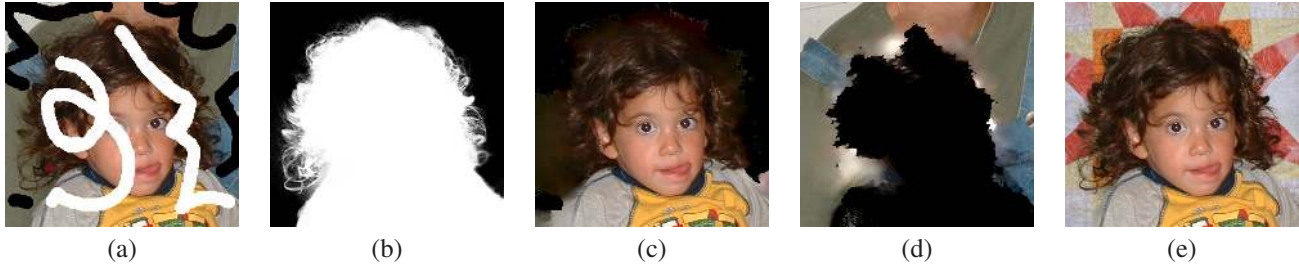


Figure 11. Foreground and background reconstruction: (a) input (b)  $\alpha$ -matte (c) foreground reconstruction (d) background reconstruction (e)  $F$  composited over a novel background.

required. Figure 11 shows an  $\alpha$ -matte and  $F$  and  $B$  images recovered in this way.

## 8. Results

In all examples presented in this section the scribbles used in our algorithm are presented in the following format: black and white scribbles are used to indicate the first type of hard constraints on  $\alpha$ . Red scribbles represent places in which foreground and background colors were explicitly specified. Finally, gray scribbles are used to represent the third type of constraint — requiring  $a$  and  $b$  to be constant (without specifying their exact value) within the scribbled area.

### 8.1. Comparisons

Figure 12 presents matting results on images from the Bayesian matting work [6]. Our results appear visually comparable to those produced by Bayesian matting. While the Bayesian matting results use a trimap, each of our results was obtained using a sparse set of scribbles.

In figure 13 we extract mattes from a few of the more challenging examples presented in the Poisson matting paper [15]. For comparison, the Poisson and Bayesian matting results provided in [15] are also shown<sup>1</sup>.

Figure 14 shows the mattes extracted using our technique on two challenging images used in [17] and compares our results to several other recent algorithms. It can be seen that our results on these examples are comparable in terms of visual quality to those of [17], even though we use a far simpler algorithm. Global Poisson matting cannot extract a good matte from a sparse set of scribbles although its performance with a trimap is quite good. The random walk matting algorithm [8] also minimizes a Laplacian but uses an affinity function with a global scaling parameter and hence has a particular difficulty with the peacock image.

Figure 15 shows an example (from [17]), where Wang and Cohen’s method fails to extract a good matte from sparse scribbles due to color ambiguity between the foreground and the background. The same method, however, is able to produce an acceptable matte when supplied with a trimap. Our method produces a cleaner, but also imperfect matte from the same set of scribbles, but adding a small

number of additional scribbles results in a better matte. (To produce this result, we applied the thresholding trick mentioned in section 6.)

Figure 16 shows another example (a closeup of the Koala image from [15]), where there’s an ambiguity between foreground and background colors. In this case the matte produced by our method is clearly better than the one produced by the Wang-Cohen method. To better understand why this is the case, we show an RGB histogram of representative pixels from the  $F$  and  $B$  scribbles. Some pixels in the background fit the foreground color model much better than the background one (one such pixel is marked red in 16(b) and indicated by an arrow in 16(d)). As a result such pixels are classified as foreground with a high degree of certainty in the first stage. Once this error has been made it only reinforces further erroneous decisions in the vicinity of that pixel, resulting in a white clump in the alpha matte.

Since our method does not make use of global color models for  $F$  and  $B$  it can handle ambiguous situations such as that in Figure 16. However, there are also cases where our method fails to produce an accurate matte for the very same reason. Figure 17 shows an actress in front of a background with two colors. Even though the black  $B$  scribbles cover both colors the generated matte includes parts of the background (between the hair and the shoulder on the left). In such cases, the user would have to add another  $B$  scribble in that area.

Figure 18 presents compositing examples using our algorithm for some images from the previous experiments. We show compositing both over a constant background and over natural images.

#### 8.1.1 Quantitative Comparisons

To obtain a quantitative comparison between the algorithms, we performed an experiment with synthetic composites for which we have the ground truth alpha matte. We randomly extracted 2000 subimages from the image shown in figure 19(h). We used each subimage as a background and composited over it a uniform foreground image using two different alpha mattes: the first matte is a computer simulated smoke most of which is partially transparent; the other matte is a part of a disk, mostly opaque

<sup>1</sup>We thank Leo Jia for providing us with the images and results

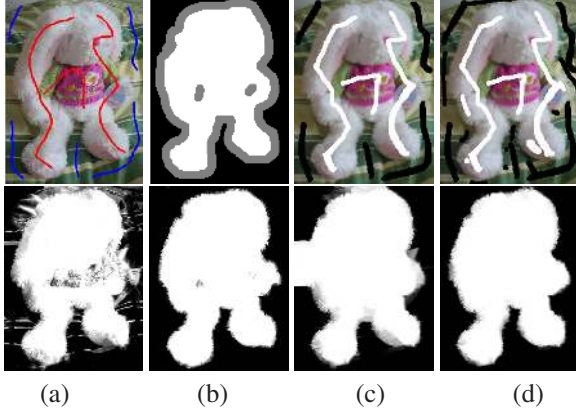
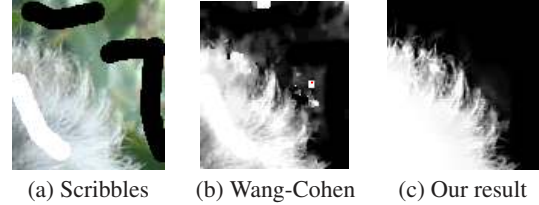


Figure 15. An example (from [17]) with color ambiguity between foreground and background. (a) scribbles and matte by [17]; (b) [17] results using a trimap; (c) our result with scribbles similar to those in (a); (d) our results with a few additional scribbles.

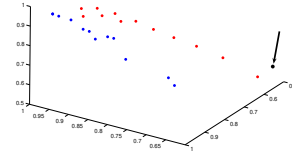
with a feathered boundary. The mattes are shown in figure 19(c). Consequently, we obtained 4000 composite images, two of which are shown in figure 19(a.) On this set of images we compared the performance of four matting algorithms: Wang and Cohen, global Poisson matting, random walk matting, and our own (using  $3 \times 3$  windows with no pyramid). All algorithms were provided a trimap as input. Examples of the trimaps and the results produced by the different methods are shown in figure 19(a,d–g)). For each algorithm, we measured the summed absolute error between the extracted matte and the ground truth. Figures 19(i,j) plot the average error of the four algorithms as a function of the smoothness of the background (specifically we measured the average gradient strength, binned into 10 bins). The errors in the smoke matte are plotted in figure 19(i), while errors in the disk matte are plotted in figure 19(j). When the background is smooth, all algorithms perform well with both mattes. When the background contains strong gradients, global Poisson matting performs poorly (recall that it assumes that background and foreground gradients are negligible). Of the remaining algorithms, our algorithm consistently produced the most accurate results.

## 8.2. Shadow Matting

Finally, figure 20 presents additional applications of our technique. In particular, the red scribbles specifying the foreground and background color, can be used to extract shadow and smoke. In the top figure, the red scribble on the shadow specifies that the foreground color is black. In the bottom figure, the red scribble on the smoke indicates the foreground color is white (in both cases the background color in the red scribbles was copied from neighboring, uncovered pixels). These sparse constraints on the  $\alpha$  were then propagated to achieve the final matte. Note that shadow matting can not be directly achieved with matting algorithms which initialize foreground colors using neighboring pixels, since no neighboring black pixels are present.



(a) Scribbles (b) Wang-Cohen (c) Our result



(d) RGB histogram of  $F$  (red) and  $B$  (blue) pixels.

Figure 16. An example with ambiguity between  $F$  and  $B$ .



Figure 17. Failure due to lack of a color model.

Note also that the shadow area captures a significant amount of the image area and it's not clear how to specify a good trimap in this case. The smoke example was processed also in [5], but in their case a background model was calculated using multiple frames.

An alternative approach for shadow extraction is to use the shadow composition equation proposed by [7]

$$I = \beta L + (1 - \beta)S$$

Where  $I$  is the input image,  $L$  the *lit image*,  $S$  the *shadow image* and  $\beta$  the *shadow density matte*. We consider the image in figure 21. We first place black and white scribbles on the man and extract him from the background. We are then left with the background image in fig 21(c) from which we would like to extract the shadow. This enables us to place black scribbles inside the shadow area and white scribbles outside. Those scribbles are used for computing the shadow mask  $\beta$  in fig. 21(d). We can use the two mattes (fig 21(b,d)) to paste both the man and his shadow within a novel scene, as shown in fig. 21(e). The double composition follows the following formula:

$$I_{new} = \alpha F + (1 - \alpha)(1 - s + s\beta B_{new})$$

where  $s$  is some scalar  $0 < s < 1$  controlling the shadow strength. To the best of our knowledge, this is the first attempt to address shadow matting using an interactive interface.

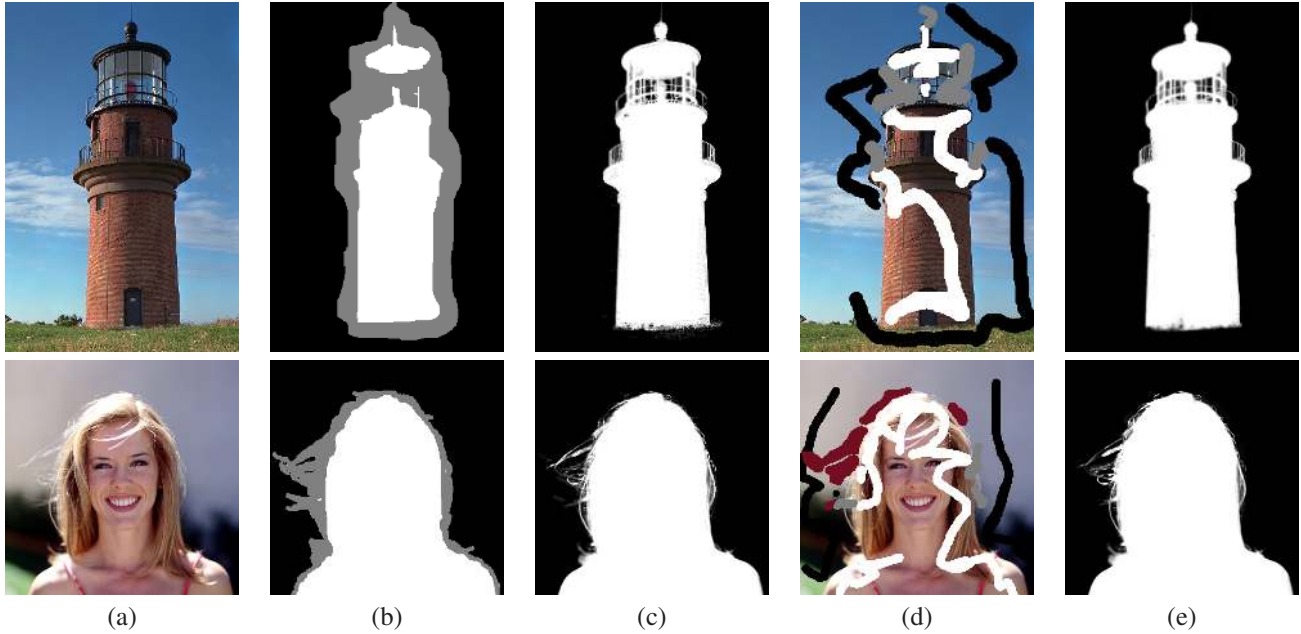


Figure 12. Result on Bayesian matting examples. (a) input image (b) trimap (c) Bayesian matting result (obtained from the Bayesian Matting webpage) (d) scribbles (e) our result.

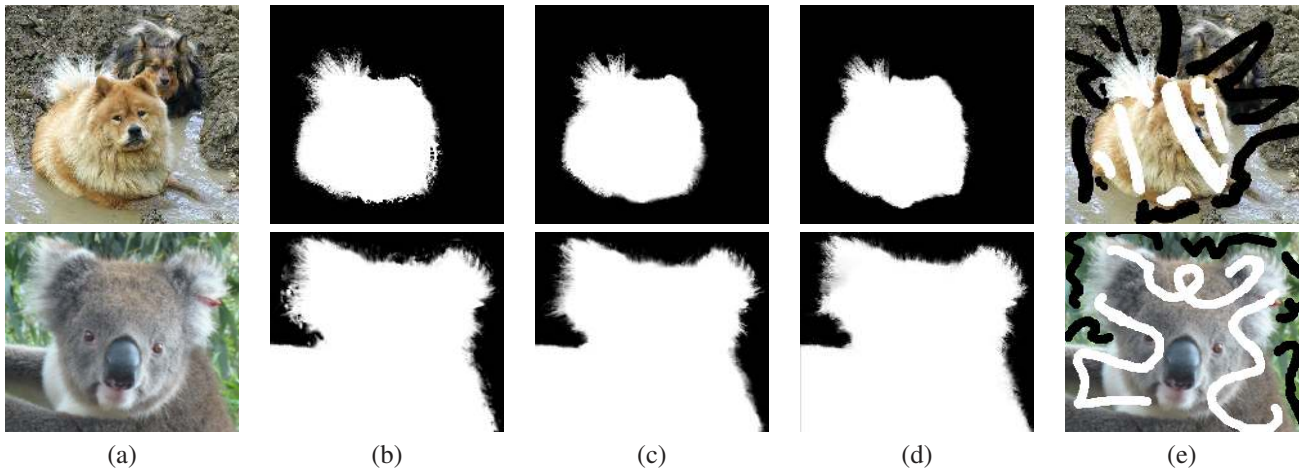


Figure 13. Result on Poisson matting examples. (a) input image (b) Bayesian matting (obtained from the Poisson matting paper) (c) Poisson matting (obtained from the Poisson matting paper) (d) our result (e) scribbles

## 9. Discussion

Matting and compositing are tasks of central importance in image and video editing and pose a significant challenge for computer vision. While this process by definition requires user interaction, the performance of most existing algorithms deteriorates rapidly as the amount of user input decreases. In this paper, we have introduced a cost function based on the assumption that foreground and background colors vary smoothly and showed how to analytically eliminate the foreground and background colors to obtain a quadratic cost function in  $\alpha$ . The resulting cost function is similar to cost functions obtained in spectral methods to image segmentation but with a novel affinity function

that is derived from the formulation of the matting problem. The global minimum of our cost can be found efficiently by solving a sparse set of linear equations. Our experiments on real and synthetic images show that our algorithm clearly outperforms other algorithms that use quadratic cost functions which are not derived from the matting equations. Furthermore, our results are competitive with those obtained by much more complicated, nonlinear, cost functions. However, compared to previous nonlinear approaches, we can obtain solutions in a few seconds, and we can analytically prove properties of our solution and provide guidance to the user by analyzing the eigenvectors of our operator.

While our approach assumes smoothness in foreground

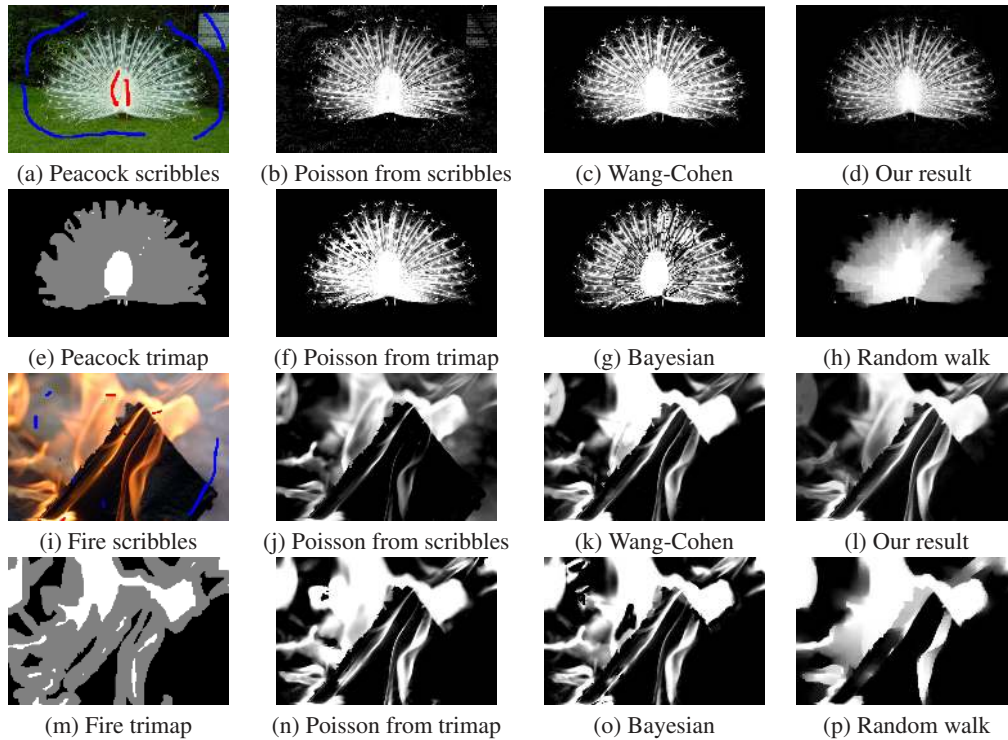


Figure 14. A comparison of alpha mattes extracted by different algorithms. Images (a,c,e,g,i,k,m,o) are taken from [17]. The remaining images were generated by our own implementation of the respective methods.

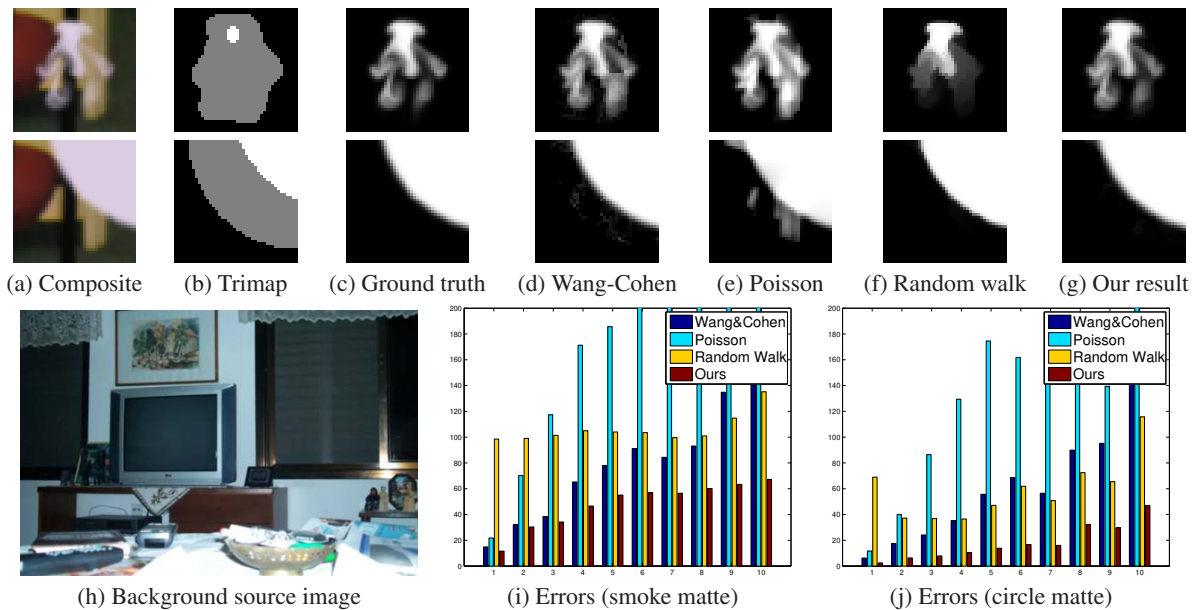


Figure 19. A quantitative comparison using two ground truth mattes. The errors in (i) and (j) are plotted as a function of average gradient strength of the background, binned into 10 bins. To produce these results we used our own implementation of the respective methods, using the parameter values specified in the original papers.

and background colors, it does not assume a global color distribution for each segment. Our experiments have demonstrated that our local smoothness assumption often

holds for natural images. Nevertheless, it would be interesting to extend our formulation to include additional assumptions on the two segments (e.g., global models, local texture

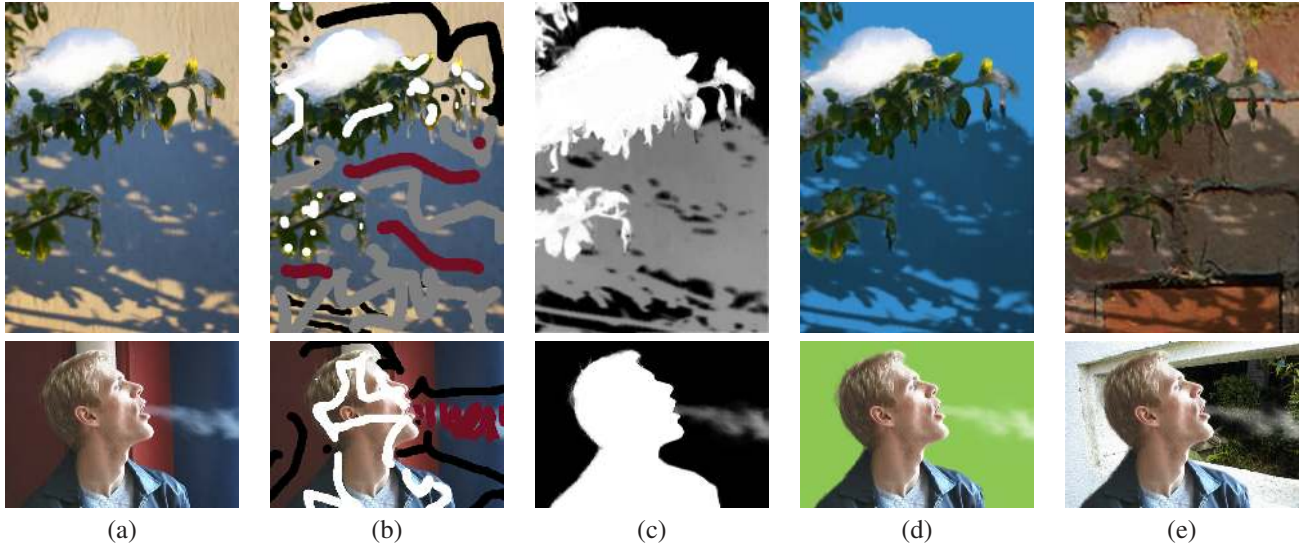


Figure 20. Additional examples. Our technique applied for shadow and smoke extraction. (a) input image (b) scribbles (c) extracted matting (d-e) compositions.

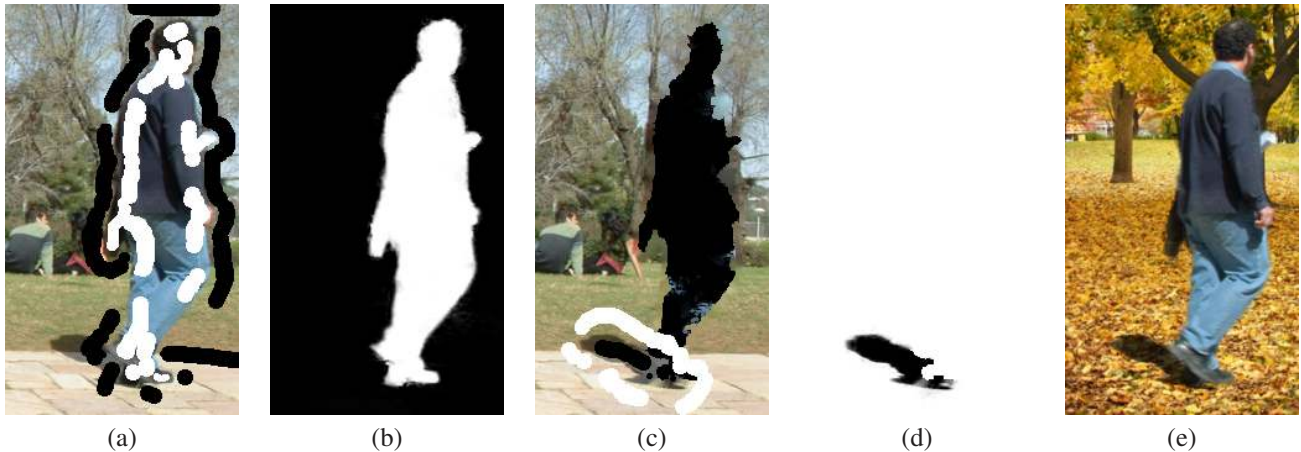


Figure 21. Shadow compositing using the [7] shadow composition equation. (a) scribbled input image (b) extracted  $\alpha$ -matte (c) extracted background with scribbled shadow (d)  $\beta$  shadow matte. (e) compositing foreground and shadow with a novel background.

models, etc.). The goal is to incorporate more sophisticated models of foreground and background but still obtain high quality results using simple numerical linear algebra.

Finally, the implementation of our matting algorithm and all examples presented in this paper are available for public usage at [www.cs.huji.ac.il/~alevin/matting.tar.gz](http://www.cs.huji.ac.il/~alevin/matting.tar.gz)

## References

- [1] N. E. Apostoloff and A. W. Fitzgibbon. Bayesian video matting using learnt image priors. In *Proc. CVPR*, 2004.
- [2] A. Berman, P. Vlahos, and A. Dadourian. Comprehensive method for removing from an image the background surrounding a selected object. US Patent no. 6,135,345, 2000.
- [3] Y. Boykov and M. P. Jolly. Interactive graph cuts for optimal boundary & region segmentation of objects in n-d images. In *Proc. ICCV*, 2001.
- [4] C. Chennubhotla and A. Jepson. Hierarchical eigensolver for transition matrices in spectral methods. In L. K. Saul, Y. Weiss, and L. Bottou, editors, *Advances in Neural Information Processing Systems 17*, pages 273–280. MIT Press, Cambridge, MA, 2005.
- [5] Y. Chuang, A. Agarwala, B. Curless, D. Salesin, and R. Szeliski. Video matting of complex scenes. *ACM Trans. Graph.*, 21(3):243–248, 2002.
- [6] Y. Chuang, B. Curless, D. Salesin, and R. Szeliski. A Bayesian approach to digital matting. In *Proc. CVPR*, 2001.
- [7] Y. Chuang, D. Goldman, B. Curless, D. Salesin, and R. Szeliski. Shadow matting and compositing. *ACM Trans. Graph.*, 2003.
- [8] L. Grady, T. Schiwietz, S. Aharon, and R. Westermann. Random walks for interactive alpha-matting. In *Proc. VIIPO5*.
- [9] A. Levin, D. Lischinski, and Y. Weiss. Colorization using optimization. *ACM Transactions on Graphics*, 2004.
- [10] Y. Li, J. Sun, C.-K. Tang, and H.-Y. Shum. Lazy snapping. *ACM Trans. Graph.*, 23(3):303–308, 2004.

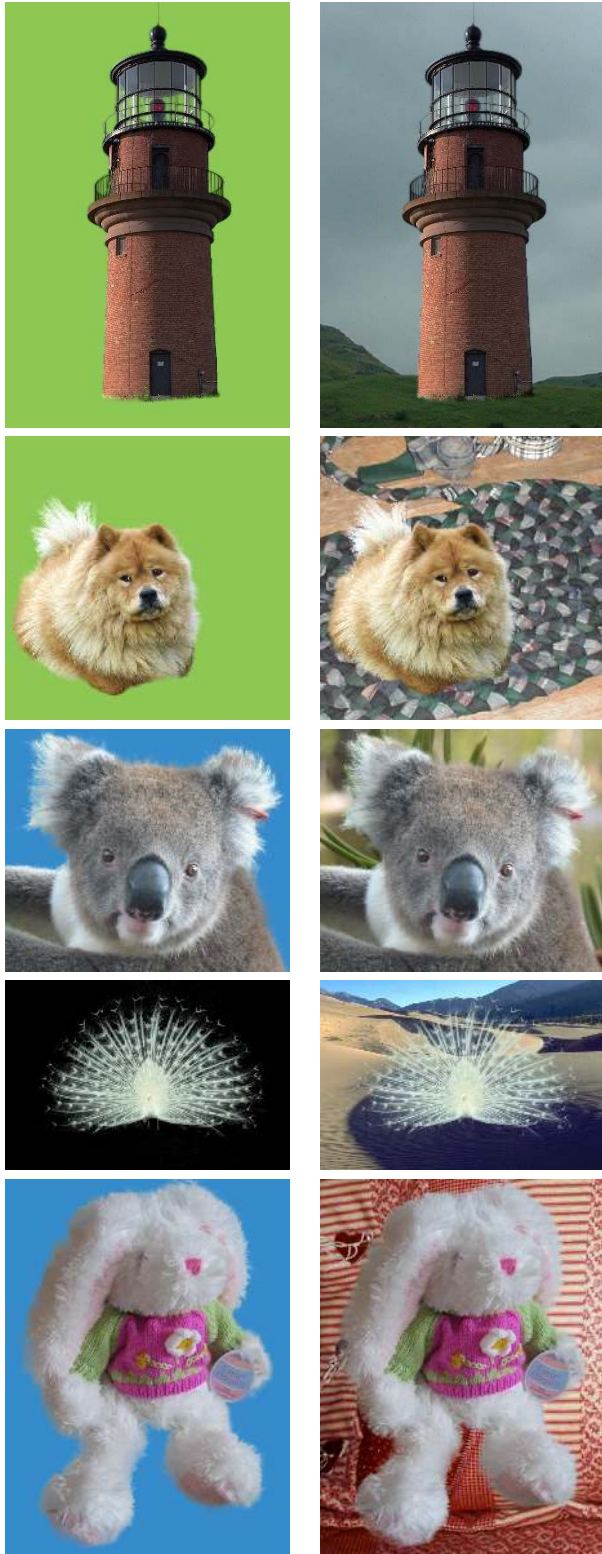


Figure 18. Some composition examples using  $\alpha$ ,  $F$  and  $B$  extracted by our algorithm. Left: compositing with a constant background. Right: natural images compositing.

- [11] I. Omer and M. Werman. Color lines: Image specific color representation. In *Proc. CVPR*, June 2004.
- [12] C. Rother, V. Kolmogorov, and A. Blake. "grabcut": interactive foreground extraction using iterated graph cuts. *ACM Trans. Graph.*, 23(3):309–314, 2004.
- [13] M. Ruzon and C. Tomasi. Alpha estimation in natural images. In *Proc. CVPR*, 2000.
- [14] J. Shi and J. Malik. Normalized cuts and image segmentation. In *Proc. CVPR*, pages 731–737, 1997.
- [15] J. Sun, J. Jia, C.-K. Tang, and H.-Y. Shum. Poisson matting. *ACM Trans. Graph.*, 23(3):315–321, 2004.
- [16] A. Torralba and W. T. Freeman. Properties and applications of shape recipes. In *Proc. CVPR*, June 2003.
- [17] J. Wang and M. Cohen. An iterative optimization approach for unified image segmentation and matting. In *Proc. IEEE Intl. Conf. on Computer Vision*, 2005.
- [18] L. Zelnik-Manor and P. Perona. Self-tuning spectral clustering. In *Advances in Neural Information Processing Systems 17*. 2005.
- [19] A. Zomet and S. Peleg. Multi-sensor super resolution. In *Proceedings of the IEEE Workshop on Applications of Computer Vision*, 2002.